

# Optical Control of Millimeter-wave Lateral Double-Drift Region Silicon IMPATT Device

Aritra ACHARYYA<sup>1</sup>, Suranjana BANERJEE<sup>2</sup>, J. P. BANERJEE<sup>1</sup>

<sup>1</sup>Inst. of Radio Physics and Electronics, University of Calcutta, 92, APC Road, Kolkata 700009, India

<sup>2</sup>Academy of Technology, West Bengal University of Technology, Adisaptagram, Hooghly 712121, West Bengal, India

ari\_besu@yahoo.co.in, suranjanarpe21@yahoo.co.in, jpbanerjee06@rediffmail.com

**Abstract.** *The effect of optical illumination on lateral Double-Drift Region (DDR) structure of Silicon Impact Avalanche Transit Time (IMPATT) device is investigated in this paper. The device is designed to operate at mm-wave W-band frequency. The optical modulation of DC and RF properties of lateral DDR IMPATT device is studied by a simulation technique which incorporates the dependence of normalized difference of photocurrent density at the depletion layer edges on the intensity of optical illumination and surface density of photon flux. The simulation results are compared with those obtained for a conventional vertical DDR Si IMPATT structure under similar optical and electrical operating conditions. The results show that the optical control is more effective in lateral IMPATT structure than in its vertical counterpart as regards reduction of output power and shifting of optimum frequency. When light is incident on hole drift layer of the lateral structure the output power reduces by 18.7% while the optimum frequency shifts upwards by 2.48%. Under similar conditions the power reduces by 10.9% and optimum frequency shifts upwards by 0.75% in vertical structure.*

## Keywords

Lateral IMPATT structure, optical control, millimeter-wave, DDR device.

## 1. Introduction

Impact Avalanche Transit Time (IMPATT) device has emerged as the most suitable solid-state source to generate sufficiently high power in microwave, millimeter-wave and terahertz frequencies [1-4]. Various types of vertical IMPATT structures like mesa, planar and distributed etc. have been reported [5-7], in which the contact and drift regions are stacked perpendicular to the substrate surface. The major disadvantage of vertical orientation is the difficulty in coupling optical energy into the active region of the device. Integration of vertical IMPATT structure in monolithic circuits is also difficult. Moreover series combination of these devices in power combiner circuits requires special technological skill. The above

problems can be resolved if the vertical IMPATT structures are replaced by lateral ones since the planar lateral IMPATT structure has the inherent advantages of monolithic integration and series combination. Stabile et al. [8] reported two types of fabrication schemes (diffused and buried geometry) for lateral Single-Drift Region (SDR)  $p^+n-n^+$  structure of IMPATT diodes and measured their RF characteristics up to a frequency of 17.4 GHz. Later Attar et al. [9-12] realized lateral SDR IMPATT diode in 0.18  $\mu\text{m}$  standard complementary metal-oxide-semiconductor (CMOS) technology so that the device can operate up to 77 GHz. These results establish the fact that lateral IMPATT structure is highly suitable for RF power generation at microwave and millimeter-wave frequency bands. Further light energy of appropriate wavelength incident on the active region of IMPATT devices leads to various optical control functions such as modulation of RF power, frequency tuning and injection locking [13-28]. The optical control provides additional control over normal electronic control and is of considerable research interest in view of its application in optoelectronic integrated circuits and phased array antennas for space based communication and imaging. The physical mechanism underlying the above control functions is the enhancement of leakage current entering in a photo-illuminated reverse biased IMPATT device.

The theoretical and experimental studies on optical control have been carried out on the conventional vertical structure of SDR or DDR IMPATT devices. The authors proposed a novel lateral DDR IMPATT structure (Fig. 1) in an earlier paper [29] in which the contact layers ( $p^+$ - and  $n^+$ -layers) and drift layers ( $p$ - and  $n$ -epitaxial layers) are adjacent to the substrate surface. Light energy can be very easily coupled to either  $p$ - or  $n$ -drift layers of the lateral DDR structure through tiny holes created on the  $\text{SiO}_2$  layer. The lateral DDR IMPATT structure shown in Fig. 1 can be fabricated by using standard CMOS technology [29]. So far as the authors' knowledge is concerned, no theoretical or experimental investigation is available in published literature on the optical control properties of lateral DDR IMPATTs. The authors have made an attempt in this paper to study the optical modulation of RF properties of proposed lateral and conventional vertical structures of IMPATTs. Simulation study is carried out to investigate

the optical control performance of lateral DDR Si IMPATT device designed to operate at 94 GHz window frequency at W-band. Two different optical illumination configurations are considered in this study. In one configuration the photocurrent is electron dominated while in the other the photocurrent is hole dominated. Similar study has been carried out on a vertical DDR Si IMPATT device under same optical and electrical operating conditions at W-band for the sake of comparison.

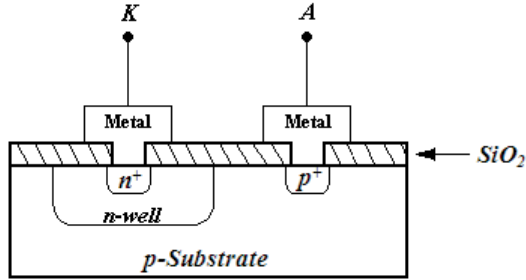


Fig. 1. Lateral DDR IMPATT structure.

## 2. Material Parameters and Design Methodology

In this section the material parameters of the base semiconductor material (silicon) and the design methodology of 94 GHz DDR IMPATT device is briefly discussed.

### 2.1 Material Parameters

The realistic field dependence of ionization rates ( $\alpha_n$ ,  $\alpha_p$ ) and drift velocities ( $v_n$ ,  $v_p$ ) of charge carriers and other material parameters such as bandgap ( $E_g$ ), intrinsic carrier concentration ( $n_i$ ), effective density of states of conduction and valance bands ( $N_c$ ,  $N_v$ ), diffusion coefficients ( $D_n$ ,  $D_p$ ), mobilities ( $\mu_n$ ,  $\mu_p$ ) and diffusion lengths ( $L_n$ ,  $L_p$ ) of Si at realistic junction temperature of 500 K are taken from the recently published experimental reports [30-32].

### 2.2 Design Methodology

The frequency of operation of an IMPATT device essentially depends on the transit time ( $\tau_T$ ) of charge carriers to cross the depletion layer of the device. IMPATT devices having double-drift  $n^+n-p-p^+$  structure are first designed for a particular frequency ( $f_d$ ) from the transit time formula of Sze and Ryder [33] given by  $W_{n,p} = 0.37 v_{sn,sp}/f_d$ ; where  $W_{n,p}$  is the width of  $n^-$  and  $p^-$  drift region, and  $v_{sn,sp}$  is the saturation drift velocity of electrons, holes respectively. Here  $n^+$  and  $p^+$  layers are highly doped layers whose doping concentrations are taken to be  $N_{n^+} = N_{p^+} = 10^{26} \text{ m}^{-3}$ . The background doping concentrations of  $n^-$  and  $p^-$  depletion regions ( $N_D$ ,  $N_A$ ) are initially chosen according to the design frequency,  $f_d$ . The design frequency is taken to be 94 GHz at W-band in the present simulation study. Using the above design doping and structural parameters the electric field profile is obtained from a double-iterative

field maximum simulation technique reported earlier [34]. The doping parameters and corresponding structural parameters are adjusted till the simulated electric field profile just punches through the depletion layers  $W_n$ ,  $W_p$  corresponding to the design frequency,  $f_d$  at a particular biasing current density,  $J_0$ . A small-signal simulation method described in [35] is used to find out the high frequency admittance and negative resistance properties of the device. This method is based on Gummel-Blue approach [36]. The optimum frequency  $f_p$  corresponding to the peak negative conductance  $G_p$  is determined from the simulated admittance characteristics of the device. If the magnitude of  $f_p$  differs very much from  $f_d$ , the value of  $J_0$  is varied and the computer simulation program is run till the value of  $f_p$  is nearly equal to the value of  $f_d$ . The bias current density,  $J_0$  is thus fixed for a particular design frequency. Realistic doping profile for flat profile DDR IMPATT diode has been used in the present analysis. The doping profile at the interface of epitaxy and substrate (i.e.  $n^+n^-$  interface) is approximated to be error function. The doping profile near the  $p^+p^-$  interface is made realistic by suitable exponential function. The structural and doping parameters of DDR Si IMPATTs designed for operation at 94 GHz are listed in Tab. 1.

$W_n$ ( $\mu\text{m}$ )	$W_p$ ( $\mu\text{m}$ )	$N_D$ ( $\times 10^{23} \text{ m}^{-3}$ )	$N_A$ ( $\times 10^{23} \text{ m}^{-3}$ )	$N_{n^+}, N_{p^+}$ ( $\times 10^{26} \text{ m}^{-3}$ )
0.3200	0.3000	1.450	1.650	1.0

Tab. 1. Design parameters.

## 3. Proposed Analysis Model

One-dimensional model of reverse biased  $n^+n-p-p^+$  lateral DDR IMPATT structure, shown in Fig. 2 is used to simulate the DC and high frequency properties of the device under optical illumination. The physical phenomena take place in the semiconductor bulk along the symmetry axis of the DDR IMPATT devices. Thus the one-dimensional model of IMPATT devices considered in this work is justified.

### 3.1 DC and High Frequency Simulation

The DC electric field and normalized current density profiles in the depletion layer of the device are obtained from simultaneous numerical solution of fundamental device equations such as Poisson's equation, combined carrier continuity equation, current density equations and mobile space charge equation subject to appropriate boundary conditions [27]. A double-iterative field maximum simulation method described elsewhere [27], [34] is used to solve these equations and obtain the field and current density profiles. In the above mentioned simulation method, the computation starts from the field maximum near the metallurgical junction. The boundary conditions for the electric field ( $\zeta(x)$ ) at the depletion layer edges are given by

$$\xi(-x_1) = 0 \text{ and } \xi(x_2) = 0. \quad (1)$$

Similarly the boundary conditions for normalized difference of hole and electron current density,  $P(x) = (J_p(x) - J_n(x)) / J_0$  (where  $J_0 = J_p + J_n$ ) at the depletion layer edges i.e., at  $x = -x_1$  and  $x = x_2$  are given by

$$P(-x_1) = \left( \frac{2}{M_p} - 1 \right) \text{ and } P(x_2) = \left( 1 - \frac{2}{M_n} \right) \quad (2)$$

where  $M_n$  and  $M_p$  are the electron and hole multiplication factors whose values are infinitely large of the order of  $\sim 10^6$  under dark or un-illuminated condition of the device.

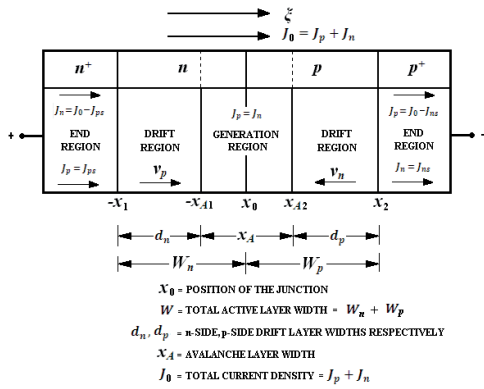


Fig. 2. One-dimensional model of DDR IMPATT device.

The magnitude of peak field at the junction  $\zeta_p$ , the widths of avalanche and drift zones ( $x_A$  and  $x_D$ ; where  $x_D = d_n + d_p$ ) and the voltage drops across these zones  $V_A$ ,  $V_D$  are obtained from the DC simulation program. These values are fed back as input parameters in the small-signal simulation to obtain the high frequency admittance properties of the device. The depletion layer edges of the device are obtained from the output of DC simulation program. The edges of the depletion layer are then taken as the starting and end points of small-signal simulation program. Two second order differential equations are framed from Gummel-Blue model [35] by resolving the device impedance  $Z(x, \omega)$  into its real part  $R(x, \omega)$  and imaginary part  $X(x, \omega)$ ; where  $Z(x, \omega) = R(x, \omega) + jX(x, \omega)$ . Two simultaneous second order differential equations in  $R$  and  $X$  are numerically solved by using Runge-Kutta method [35]. Double-iteration over the initial choice of the values of  $R$  and  $X$  at one edge is carried out till the boundary conditions for  $R$  and  $X$  are satisfied at the other edge [35]. The negative specific resistance  $R(x)$  and specific reactance  $X(x)$  profiles in the depletion layer of the device are obtained from the above solution. The device negative resistance  $Z_R$  and reactance  $Z_X$  are obtained from the numerical integration of the respective  $R(x)$ - and  $X(x)$ -profiles over the depletion layer width  $W$ , i.e.

$$Z_R = \int_{-x_1}^{x_2} R(x) dx \text{ and } Z_X = \int_{-x_1}^{x_2} X(x) dx. \quad (3)$$

The device impedance is given by,  $Z_D = Z_R + jZ_X$  while the device admittance is,  $Y_D = Z_D^{-1} = G + jB$ . The negative conductance  $G$  and positive susceptance  $B$  of the device at

a particular frequency are computed from the following expressions

$$|G(\omega)| = \frac{Z_R}{(Z_R^2 + Z_X^2)} \text{ and } |B(\omega)| = \frac{-Z_X}{(Z_R^2 + Z_X^2)}. \quad (4)$$

It may be noted that both  $G$  and  $B$  are normalized with respect to the junction area  $A_j$  of the device. The admittance characteristics i.e.,  $G(\omega)$  versus  $B(\omega)$  plots of the device are obtained from the above analysis for different bias current densities. The avalanche resonance frequency  $f_a$  at which the susceptance  $B$  changes its sign from positive to negative i.e., from inductive to capacitive is also obtained from the admittance plots.

### 3.2 Proposed Model to Study the Optical Control of Lateral DDR IMPATT Device

The optical energy can be fed to the ring contact of conventional vertical mesa structure of IMPATT device by shining light through a controlled optical window on either  $p^+$ -layer (to generate electron dominated photocurrent) or  $n^+$ -layer (to generate hole dominated photocurrent) [13], [14], [26], [27]. Although simple to describe, the method of shining light on the top surface of the device is technologically complex. Further it is difficult to shine light through the controlled optical window on the vertical structure of DDR IMPATT device in the experimental set up described in [9]. However light may easily be fed directly to the  $n$ - or  $p$ -drift layers through tiny holes created on the  $\text{SiO}_2$ -layer in lateral structure of DDR IMPATTs as shown in Fig. 3 [29]. In this section studies will be presented on the optical control of high frequency properties of DDR Si lateral IMPATT device. The effect of variation of intensity of optical illumination corresponding to different incident photon flux densities on the optical control phenomena of lateral device structure is also investigated. The device is designed to operate at W-band around the window frequency of 94 GHz. An analytical relation between incident photon flux and the normalized difference of electron and hole photocurrent density at the depletion layer edges is derived and incorporated in the simulation program to study the above phenomena.

If the incident optical power be  $P_{in}$  watts and the effective illumination area of the device be  $A$ , then the surface density of photon flux  $\Phi_0$  is given by

$$\Phi_0 = P_{in} \frac{(1 - R(\lambda))\lambda}{Ahc} \quad (5)$$

where  $R(\lambda)$  is the reflectance ( $R = (n_2 - n_1) / (n_2 + n_1)$ );  $n_2$  is the refractive index of the semiconductor,  $n_1$  is the refractive index of air) of the semiconductor material at wavelength  $\lambda$ ,  $h$  is Planck's constant ( $h = 6.625 \times 10^{-34}$  Js) and  $c$  is the velocity of light in vacuum ( $c = 3 \times 10^8$  ms $^{-1}$ ). In the present analysis, the device thickness  $D$  (effectively  $n$ -well depth) is assumed to be much larger than the light penetration depth ( $\delta = 1/\alpha$  where  $\alpha$  is the absorption coefficient of the semiconductor material) and the incident optical power

is assumed to be completely absorbed within the active layer. Under the above assumptions, the steady-state optical generation rate of carriers within the  $n$ - or  $p$ -drift layer of lateral DDR IMPATT device is given by

$$G_L' = \left( \frac{\eta_{int}}{WLD} \right) \left( \frac{P_{in}\lambda}{hc} \right) \quad (6)$$

where  $\eta_{int}$  is the internal quantum efficiency,  $W$  and  $L$  are respectively the width and length of the hole created on SiO<sub>2</sub>-layer to allow light to be incident directly on either  $n$ - or  $p$ -drift layers. If light is incident on  $n$ -layer,  $L = W_n = (|-x_1| - x_0)$ . On the other hand if light is incident on  $p$ -layer, then  $W_p = (x_2 - x_0)$ . The electron and hole current multiplication factors at the  $n$ - and  $p$ -depletion layer edges are given by

$$M_n = \frac{J_0}{J_{lat\ ns(Total)}} \quad \text{and} \quad M_p = \frac{J_0}{J_{lat\ ps(Total)}} \quad (7)$$

where  $J_{lat\ ns/ps(Total)}$  is the total electron/hole reverse saturation current entering the lateral DDR IMPATT structure of the device under optical illumination. The electron and hole reverse saturation currents have two components, (a) thermally generated saturation current and (b) optically generated saturation current. Thus:

$$\left. \begin{aligned} J_{lat\ ns(Total)} &= J_{lat\ ns(Th)} + J_{lat\ ns(Opt)} \\ &\text{and} \\ J_{lat\ ps(Total)} &= J_{lat\ ps(Th)} + J_{lat\ ps(Opt)} \end{aligned} \right\} \quad (8)$$

The expressions for thermally generated electron and hole reverse saturation currents are given by:

$$J_{ns(Th)} = \left[ \frac{qD_n n_i^2}{L_n N_A} \right] \quad \text{and} \quad J_{ps(Th)} = \left[ \frac{qD_p n_i^2}{L_p N_D} \right] \quad (9)$$

where  $q$  is the unit electronic charge ( $q = 1.6 \times 10^{-19}$  C). Under dark condition,  $J_{lat\ ns(Opt)} = J_{lat\ ps(Opt)} = 0$ , so the magnitudes of current multiplication factors  $M_n$  and  $M_p$  are of the order of  $\sim 10^6$  [26].

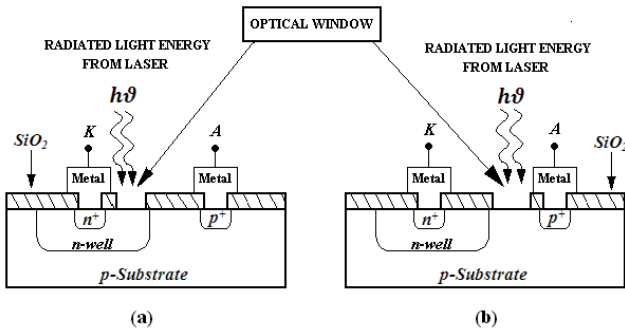


Fig. 3. Arrangement for optical illumination on (a)  $n$ -drift and (b)  $p$ -drift layers of Lateral DDR IMPATT structure.

The drift component of the photocurrent density due to light incident through tiny holes created on the SiO<sub>2</sub>-

layer directly on the  $n$ -drift layer of lateral DDR IMPATTs is given by

$$J_{lat\ ns(Opt\_drift)} = q \int_{|-x_1|}^{x_0} G_L' dx = q \left( \frac{\eta_{int}}{WLD} \right) \left( \frac{P_{in}\lambda}{hc} \right) W_n \quad (10)$$

Similarly, the drift component of the photocurrent density due to light incident directly on the  $p$ -drift layer of the device is given by

$$J_{lat\ ps(Opt\_drift)} = q \int_{x_0}^{x_2} G_L' dx = q \left( \frac{\eta_{int}}{WLD} \right) \left( \frac{P_{in}\lambda}{hc} \right) W_p \quad (11)$$

Diffusion components of the photo current density in both  $n^+$ - and  $p^+$ -layers can separately be determined by solving one-dimensional ambipolar transport equation with proper boundary conditions [37]. The electron and hole diffusion components of the photo current density in  $n^+$ - and  $p^+$ -layers are given by

$$\left. \begin{aligned} J_{lat\ ns(Opt\_diff)} &= qG_L' L_n = q \left( \frac{\eta_{int}}{WLD} \right) \left( \frac{P_{in}\lambda}{hc} \right) L_n \\ &\text{and} \\ J_{lat\ ps(Opt\_diff)} &= qG_L' L_p = q \left( \frac{\eta_{int}}{WLD} \right) \left( \frac{P_{in}\lambda}{hc} \right) L_p \end{aligned} \right\} \quad (12)$$

Total photocurrent density is the combination of drift and diffusion components; i.e.

$$\left. \begin{aligned} J_{lat\ ns(Opt)} &= J_{lat\ ns(Opt\_drift)} + J_{lat\ ns(Opt\_diff)} \\ &\text{and} \\ J_{lat\ ps(Opt)} &= J_{lat\ ps(Opt\_drift)} + J_{lat\ ps(Opt\_diff)} \end{aligned} \right\} \quad (13)$$

### 3.2.1 Light Incident on $p$ -drift Layer

When light is shined on the  $p$ -drift layer of the lateral DDR IMPATT device, the photocurrent density will be electron dominated. Under this situation the electron and hole multiplication factors in the  $n$ - and  $p$ -depletion layers are given by

$$M_n'' = \frac{J_0}{J_{lat\ ns(Th)} + J_{lat\ ns(Opt)}} \quad \text{and} \quad M_p = \frac{J_0}{J_{lat\ ps(Th)}} \quad (14)$$

In this case the value of  $M_n''$  is considerably reduced ( $M_n'' \ll 10^6$ ) while  $M_p$  remains unchanged ( $\sim 10^6$ ). Therefore the boundary conditions for the normalized current density at the depletion layer edges (equation (2)) are modified as

$$P(-x_1) = -1 \quad \text{and} \quad P(x_2) = \left( 1 - \frac{2}{M_n''} \right) \quad (15)$$

When light is shined on the  $p$ -drift layer, equation (15) is used as one of the boundary conditions in place of equation (2) to solve the device equations involved in the program and simulate the DC and high frequency properties of the device.

### 3.2.2 Light Incident on $n$ -drift Layer

When light is shined on the  $n$ -drift layer of the lateral DDR structure of Si IMPATT device, the photocurrent density will be hole dominated. Under this situation the electron and hole multiplication factors in the  $n$ - and  $p$ -depletion layers are given by

$$M_n = \frac{J_0}{J_{lat\ ns(Th)}} \quad \text{and} \quad M_p'' = \frac{J_0}{J_{lat\ ps(Th)} + J_{lat\ ps(Opt)}}. \quad (16)$$

In this case the value of  $M_p''$  is considerably reduced ( $M_p'' < 10^6$ ) while  $M_n$  remains unchanged ( $\sim 10^6$ ). Thus the boundary conditions for the normalized current density at the depletion layer edges (equation (2)) are modified to

$$P(-x_1) = \left( \frac{2}{M_p''} - 1 \right) \quad \text{and} \quad P(x_2) = 1. \quad (17)$$

Thus when light is shined on the  $n$ -drift layer, equation (17) is used as one of the boundary conditions in place of equation (2) for simulating the DC and high frequency properties of the lateral DDR IMPATT device.

## 4. Results and Discussion

The effect of intensity of optical illumination with varying surface density of photon flux on the mm-wave properties of lateral DDR Si IMPATT device has been studied. The modified boundary conditions for normalized current density given in (15) or (17) corresponding to light incident on  $p$ - and  $n$ -drift layers are incorporated into the double-iterative simulation program to study the aforementioned properties of lateral structure of the device. Similar study is carried out for the conventional vertical structure of DDR Si IMPATT device under identical conditions by following the method reported earlier by the authors [27], [28] for the sake of comparison.

### 4.1 Dependence of Electron and Hole Dominated Photocurrents on Surface Density of Photon Flux

The bandgap of Si at 500 K is  $E_g = 1.0465$  eV [38] and the corresponding cut off wavelength is  $\lambda_g = 1.186$   $\mu\text{m}$  ( $\lambda_g = hc/E_g$ ). Thus incident light energy is absorbed in Si if and only if the wavelength of light is less than or equal to 1.186  $\mu\text{m}$ . This means that photons of wavelength equal to or less than 1.186  $\mu\text{m}$  are capable of generating electron-hole pairs in Si. Further it may be noted that the absorption coefficient ( $\alpha\ \text{m}^{-1}$ ) of light in Si is strongly dependent on wavelength as well as temperature [39], [40]. Electron and hole dominated photocurrents at the  $p^+p$ - and  $n^+n$ -interfaces of lateral DDR IMPATT device are determined for different surface densities of photon flux of wavelength 1000 nm (1.0  $\mu\text{m}$ ) which is close to the cut off wavelength in Si at a junction temperature of 500 K. He-Ne laser source with the arrangement of variation of intensity of

optical illumination may be used to illuminate the drift layers of the device. Analytical relations are derived to calculate electron and hole dominated photocurrents for different values of surface density of photon flux for the conventional vertical structure of 94 GHz DDR Si IMPATTs by using the method reported in [27], [28] for different surface densities of photon flux of 1000 nm wavelength ( $I_{ver\ ns(Opt)/ps(Opt)} = J_{ver\ ns(Opt)/ps(Opt)} \times A_j$ ; where junction area,  $A_j = \pi(D_j/2)^2$ , junction diameter,  $D_j = 35$   $\mu\text{m}$  at 94 GHz [41]). Also the electron and hole dominated photocurrents are calculated for 94 GHz lateral DDR Si IMPATTs by using the relation given in (13) for different surface densities of photon flux of 1000 nm wavelength ( $I_{lat\ ns(Opt)/ps(Opt)} = J_{lat\ ns(Opt)/ps(Opt)} \times A_j$ ; where  $A_j = D \times W$ ,  $n$ -well depth,  $D = 0.9$   $\mu\text{m}$  [42], width of the device,  $W = 1.1$  mm). The junction diameter of both vertical and lateral IMPATTs are taken to be same ( $A_j = A_j = 9.6211 \times 10^{-10}$   $\text{m}^2$ ) for the sake of comparison. Again the illumination area of the both lateral and vertical structures of DDR Si IMPATT devices are kept same ( $A = 3.3 \times 10^{-10}$   $\text{m}^2$ ) to compare the effects of optical control in the lateral and vertical structures of 94 GHz DDR Si IMPATT devices on the variation of intensity of optical illumination and corresponding variation of surface densities of photon flux. The internal quantum efficiency ( $\eta_{int}$ ) of Si in the depletion region of DDR IMPATTs is taken to be 95% [43]. The doping and structural parameters (Tab. 1) of both lateral and vertical structures of DDR IMPATT devices are taken to be same for the above study. The DC and high frequency parameters of both lateral and vertical DDR Si IMPATTs designed at 94 GHz for different surface densities of photon flux are obtained from the simulation software developed for this purpose [27]. In the following section, the simulation results for the effect of optical illumination on the DC and high frequency performance of lateral Si DDR IMPATTs will be presented compared with those of its vertical counterpart.

### 4.2 Effect of Optical Illumination on the DC Properties

The DC parameters of the lateral and vertical IMPATTs under dark (DR) and two illumination configurations (HDPC and EDPC: HDPC stands for hole dominated photocurrent and EDPC stands for electron dominated photocurrent) for different surface densities of photon flux of wavelength 1000 nm are evaluated and given in Tab. 2. Variations of breakdown voltage  $V_B$  and DC to RF Conversion Efficiency ( $\eta = \pi^{-1} \times (V_D/V_B)$ ) of lateral and vertical IMPATT structures with bias current density  $J_0$  for DR, EDPC and HDPC conditions are shown in Fig. 4 for different incident photon flux densities  $\Phi_0$ . It is observed from Tab. 2 and Fig. 4 that the optical modulation of millimeter wave properties both lateral and vertical structures of DDR Si IMPATTs are more pronounced for electron dominated photocurrents than for hole dominated photocurrents. The physical reason behind the phenomenon of more pronounced effect of electron dominated photocurrent in optically illuminated vertical structure of DDR Si

IMPATT device is explained in earlier papers [26-28]. Further it is interesting to note that significant optical modulation takes place in lateral DDR IMPATTs than in its vertical counterpart for both electron and hole dominated photocurrents. When the photocurrent is electron dominated and incident photon flux density is  $1.0 \times 10^{26} \text{ m}^{-2} \text{ sec}^{-1}$  at 1000 nm wavelength, the peak electric field  $\xi_p$ , breakdown voltage  $V_B$  and efficiency  $\eta$  of lateral DDR IMPATT structure are reduced by 1.5%, 2.3% and 16.7% respectively at a bias current density of  $3.0 \times 10^8 \text{ Amp/m}^2$ . The above mentioned parameters i.e.,  $\xi_p$ ,  $V_B$  and  $\eta$  of vertical DDR structure are reduced by 0.7%, 1.5% and 9.5% respectively under identical situation. This shows that better optical control is achieved in lateral DDR IMPATTs as compared to that in its vertical counterpart as regards the DC properties of the device.

### 4.3 Effect of Optical Illumination on the High Frequency Properties

The small-signal admittance and negative resistance of lateral and vertical IMPATT structures under dark (DR) and two illumination configurations (HDPC and EDPC) are simulated for different surface densities of photon flux of wavelength 1000 nm. The results are given in Tab. 3. It is observed from Tab. 3 that the small-signal parameters of lateral structure of DDR Si IMPATT device are more affected than that of its vertical counterpart by both electron and hole dominated photocurrents. It was reported earlier [19-28] that the small-signal parameters of vertical structure are affected more by electron dominated photocurrent than by hole dominated photocurrent. Tab. 3 shows that the electron dominated photocurrent due to optical illumination

Optical Illumination Conditions	$\Phi_0(\lambda)$ ( $\text{m}^{-2} \text{ sec}^{-1}$ ) ( $\lambda = 1000 \text{ nm}$ )	LATERAL IMPATT ( $J_0 = 3.0 \times 10^8 \text{ A m}^{-2}$ )			VERTICAL IMPATT ( $J_0 = 3.0 \times 10^8 \text{ A m}^{-2}$ )		
		$\xi_p$ ( $\times 10^7 \text{ V m}^{-1}$ )	$V_B$ (V)	$\eta$ (%)	$\xi_p$ ( $\times 10^7 \text{ V m}^{-1}$ )	$V_B$ (V)	$\eta$ (%)
Dark (DR)	0	6.3168	21.55	9.62	6.3168	21.55	9.62
Hole dominated photo current (HDPC)	$10^{25}$	6.2906	21.46	9.35	6.3078	21.51	9.49
	$10^{26}$	6.2656	21.35	9.11	6.2889	21.39	9.31
Electron dominated photo current (EDPC)	$10^{25}$	6.2325	21.32	8.73	6.2928	21.47	9.14
	$10^{26}$	6.2207	21.05	8.01	6.2709	21.22	8.71

Tab. 2. DC parameters of lateral and vertical DDR Si IMPATTs under dark and two illumination configurations for different photon flux densities.

Optical Illumination Conditions	$\Phi_0(\lambda)$ ( $\text{m}^{-2} \text{ sec}^{-1}$ ) ( $\lambda = 1000 \text{ nm}$ )	LATERAL IMPATT ( $J_0 = 3.0 \times 10^8 \text{ Amp/m}^2$ )					VERTICAL IMPATT ( $J_0 = 3.0 \times 10^8 \text{ Amp/m}^2$ )				
		$f_p$ (GHz)	$G_p$ ( $\times 10^7 \text{ S m}^{-2}$ )	$Q_p$ ( $= -B_p/G_p$ )	$Z_R$ ( $\times 10^{-8} \Omega \text{ m}^2$ )	$P_{RF}$ (mW)	$f_p$ (GHz)	$G_p$ ( $\times 10^7 \text{ S m}^{-2}$ )	$Q_p$ ( $= -B_p/G_p$ )	$Z_R$ ( $\times 10^{-8} \Omega \text{ m}^2$ )	$P_{RF}$ (mW)
DR	0	93.00	-6.5594	1.69	-0.3954	598.4	93.00	-6.5594	1.69	-0.3954	598.4
HDPC	$10^{25}$	93.44	-6.5017	1.72	-0.3886	579.1	93.15	-6.5298	1.70	-0.3937	589.2
	$10^{26}$	93.90	-6.4531	1.74	-0.3848	561.4	93.50	-6.5085	1.72	-0.3881	574.8
EDPC	$10^{25}$	93.99	-6.3864	1.75	-0.3854	537.2	93.29	-6.4671	1.72	-0.3906	566.4
	$10^{26}$	95.20	-6.2519	1.78	-0.3837	486.7	93.77	-6.4165	1.74	-0.3870	533.5

Tab. 3. High frequency parameters of lateral and vertical DDR Si IMPATTs under dark and two illumination configurations for different surface densities of photon flux.

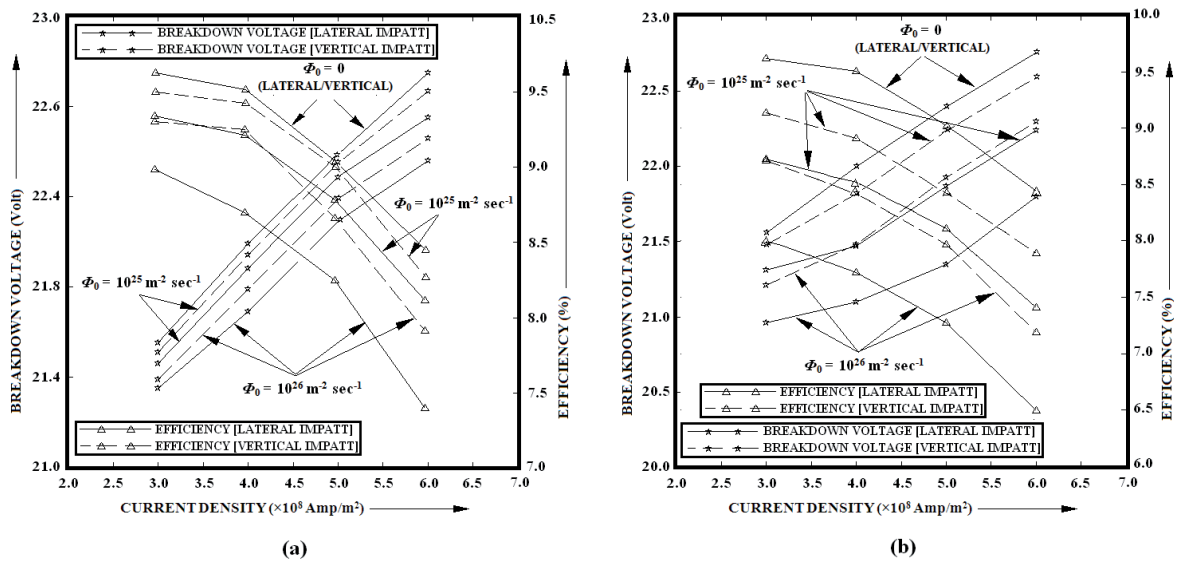


Fig. 4. Variations of breakdown voltage and DC to RF conversion efficiency with bias current density at different incident surface densities of photon flux due to (a) hole dominated and (b) electron dominated photo currents in lateral and vertical DDR Si IMPATTs ( $\lambda = 1000 \text{ nm}$ ,  $\alpha = 1.5 \times 10^4 \text{ m}^{-1}$ ,  $n_2 = 3.49713$ ).

on the vertical structure of DDR IMPATT device (incident surface density of photon flux of  $1.0 \times 10^{26} \text{ m}^{-2} \text{ sec}^{-1}$  at 1000 nm wavelength) reduces the RF power output ( $P_{RF} = \eta \times P_{DC}$ , where  $P_{DC} = V_B \times J_0 \times A_j$ ) by 10.9% and shifts the peak optimum frequency  $f_p$  up by 0.75% at the optimum bias current density of  $3.0 \times 10^8 \text{ Am}^{-2}$ . The reduction of  $P_{RF}$  and upward shift of  $f_p$  due to electron dominated photocurrent in the corresponding lateral structure are obtained as 18.7% and 2.48% respectively at the same bias current density.

The admittance characteristics of both lateral and vertical IMPATTs under dark (DR) and two illumination configurations (HDPC and EDPC) are shown in Fig. 5 for different surface densities of photon flux of wavelength 1000 nm. It is clear from both Tab. 3 and Fig. 5 that the reduction of the magnitude of negative conductance is

more by electron dominated photo current than by hole dominated photo current. Further it is observed that the effects of optical illumination on the admittance plots (Fig. 5) as well as negative resistivity profiles (Fig. 6) are more pronounced in lateral structure of DDR IMPATTs than in its vertical counterpart. Maximum decrement of the magnitude of negative resistivity for lateral IMPATT structure is nearly 3.0% whereas the same for the vertical structure is only 2.1%. From Tab. 3 and Fig. 5 it is observed that the upward frequency chirp in lateral IMPATT structure is 2.2 GHz due to optical illumination on the *p*-drift layer (incident photon flux of  $1.0 \times 10^{26} \text{ m}^{-2} \text{ sec}^{-1}$  of 1000 nm wavelength) when the photocurrent is electron dominated. The magnitude of upward frequency shift is much lower (770 MHz) in optically illuminated vertical IMPATT structure generating electron dominated photocur

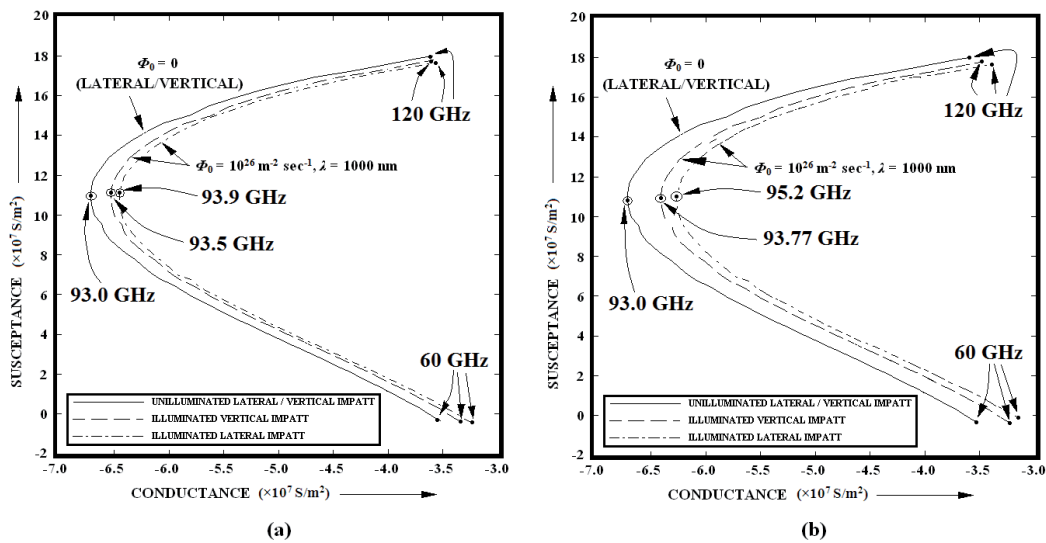


Fig. 5. Effect of (a) hole dominated and (b) electron dominated photo-currents on the admittance characteristics of the Si based lateral and vertical DDR IMPATTs ( $\lambda = 1000 \text{ nm}$ ,  $\alpha = 1.5 \times 10^4 \text{ m}^{-1}$ ,  $n_2 = 3.49713$ ).

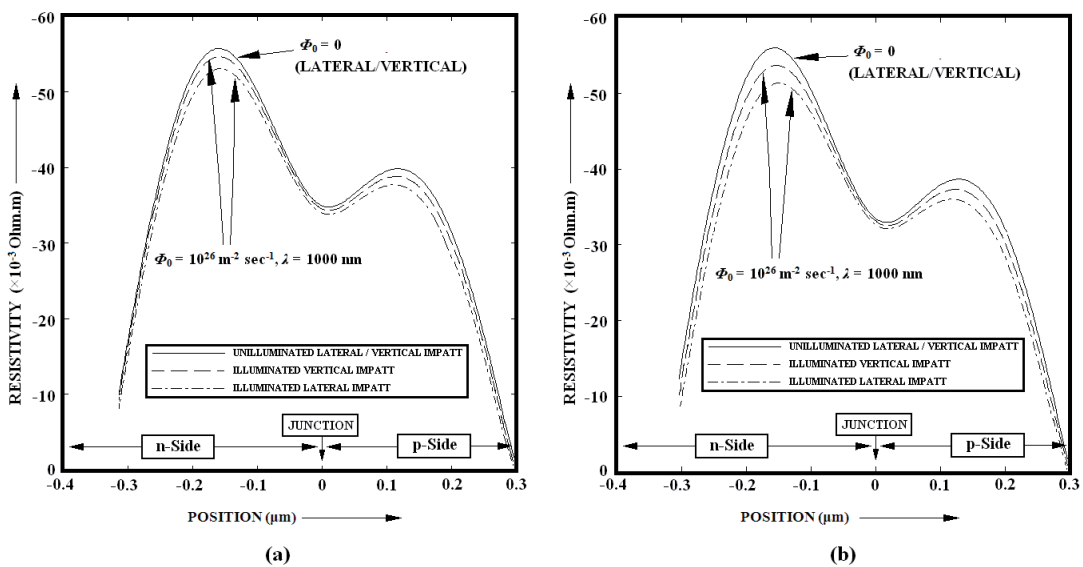


Fig. 6. Effect of (a) hole dominated and (b) electron dominated photo-currents on the negative resistivity profiles of the Si based lateral and vertical DDR IMPATTs ( $\lambda = 1000 \text{ nm}$ ,  $\alpha = 1.5 \times 10^4 \text{ m}^{-1}$ ,  $n_2 = 3.49713$ ).

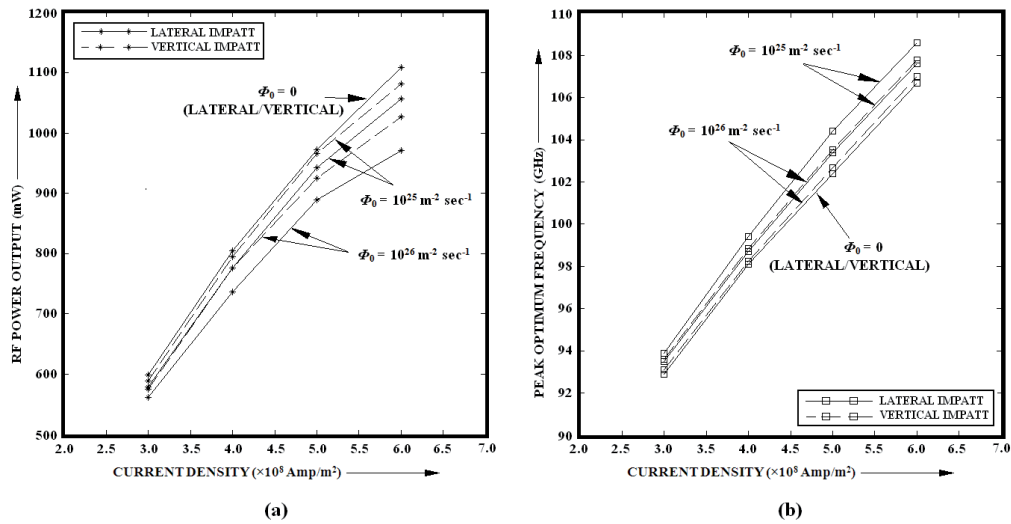


Fig. 7. Variations of (a) RF power output and (a) peak optimum frequency with bias current density at different incident surface densities of photon flux due to hole dominated photo current in lateral and vertical DDR Si IMPATTs ( $\lambda = 1000$  nm,  $\alpha = 1.5 \times 10^4$  m<sup>-1</sup>,  $n_2 = 3.49713$ ).

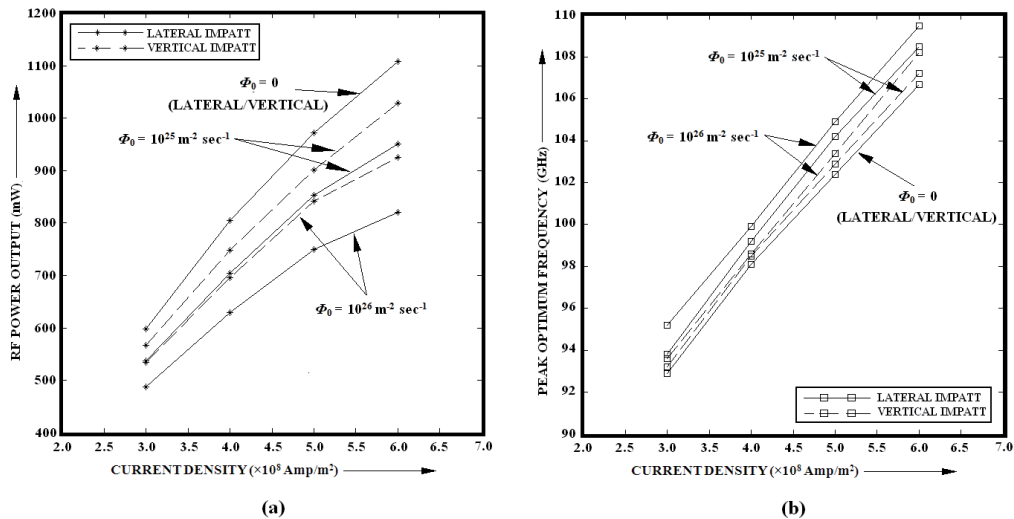


Fig. 8. Variations of (a) RF power output and (a) peak optimum frequency with bias current density at different incident surface densities of photon flux due to electron dominated photo current in lateral and vertical Si DDR IMPATTs ( $\lambda = 1000$  nm,  $\alpha = 1.5 \times 10^4$  m<sup>-1</sup>,  $n_2 = 3.49713$ ).

rent due to light incident on  $p^+$ -layer with same photon flux density and same bias current density. The variations of RF power output  $P_{RF}$  and optimum frequency  $f_p$  with bias current density are shown in Fig. 7 and Fig. 8 respectively for different photon flux densities of wavelength 1000 nm incident on lateral and vertical IMPATT structures. It is evident from the figures that the optical control is more effective in the lateral structure of DDR IMPATT device than in its vertical counterpart as regards both RF power and optimum frequency.

#### 4.4 Comparison with Experimental Results

Experimental results of optically illuminated vertical SDR structure of Si IMPATTs show that the electron dominated photocurrent is more important than the hole dominated photocurrent in modulating the DC & RF prop-

erties of the device [14]. Simulation results presented in this paper for optically illuminated vertical DDR structure of Si IMPATTs show similar behavior as that observed experimentally in case of vertical structure of SDR Si IMPATTs. The frequency tuning of IMPATT oscillators has also been experimentally demonstrated up to W-band by Seeds et al. [18]. They observed a frequency tuning of 9.4 MHz for an IMPATT oscillator operating at 91.83 GHz in which the photocurrent was measured to be 20  $\mu$ A. The simulation study presented in this paper shows that a frequency tuning in the range of 770 MHz is possible for an optically illuminated 94 GHz vertical structure of DDR Si IMPATT oscillator. Since the experimental report on the optical modulation of Si based lateral DDR Si IMPATT device at 94 GHz is not available in the published literatures, the simulation results presented in this paper can't be compared with the experimental results.

## 5. Conclusions

In this paper the effect of optical illumination on the DC and high frequency properties of 94 GHz lateral structure of DDR IMPATT device is investigated. The optical modulation of DC and RF properties of lateral DDR IMPATT device is studied by a simulation technique which incorporates the dependence of normalized difference of photocurrent density at the depletion layer edges on the intensity of optical illumination and surface density photon flux. The simulation results are compared with those of a conventional vertical structure of DDR Si IMPATT device under similar optical and electrical operating conditions. The results clearly establish that the optical control phenomenon is more effective and important in lateral DDR IMPATT device than in its vertical counterpart. The doping and structural parameters of lateral DDR structure of Si IMPATT device designed to operate at 94 GHz window are presented in this paper. These data will be highly useful to the experimentalist to fabricate the device and realize better optical control of the oscillator performance in mm-wave communication systems, optoelectronic integrated circuits and phased array antennas.

## References

- [1] MIDFORD, T. A., BERNICK, R. L. Millimeter wave CW IMPATT diodes and oscillators. *IEEE Trans. Microwave Theory Tech.*, 1979, vol. 27, no. 5, p. 483-492.
- [2] ACHARYYA, A., MUKHERJEE, M., BANERJEE, J. P. Studies on the millimeter-wave performance of MITATTs from avalanche transit time phase delay. In *IEEE Applied Electromagnetics Conference 2011*. Kolkata (India), December 18-22, 2011.
- [3] ACHARYYA, A., MUKHERJEE, M., BANERJEE, J. P. Influence of tunnel current on DC and dynamic properties of silicon based terahertz IMPATT source. *Terahertz Science and Technology*, 2011, vol. 4, no. 1, p. 26-41.
- [4] ACHARYYA, A., BANERJEE, J. P. Potentiality of IMPATT devices as terahertz source: An avalanche response time based approach to determine the upper cut-off frequency limits. *IETE Journal of Research*. Accepted, to be published March-April 2013.
- [5] JOHNSTON, R. L., DE LOACH, D. C., COHEN, B. G. A silicon diode microwave oscillator. *Bell Syst. Tech. J. Briefs*, 1965, vol. 44, p. 369-372.
- [6] LEE, D. H., WELLER, K. P., THROWER, W. F. Ion-implanted planar mesa IMPATT diodes for millimeter wavelengths. *IEEE Trans. on Electron. Devices*, 1978, vol. 25, p. 714-722.
- [7] MIDFORD, T. A., BOWERS, H. C. A two-port IMPATT diode travelling wave amplifier. *Proc. of IEEE*, 1968, vol. 56, p. 1724 to 1725.
- [8] STABILE, P. J., LALEVIC, B., Lateral IMPATT diodes. *IEEE Trans. on Electron devices*, 1989, vol. 10, no. 6, p. 249-251.
- [9] AL-ATTAR, T., MULLIGAN, M., LEE, T. H. Lateral IMPATT diodes in standard CMOS technology. In *Int. Electron Devices Meeting Dig.* Washington, DC, Dec. 13-14, 2004, p. 459 to 462.
- [10] AL-ATTAR, T., MULLIGAN, M., LEE, T. H. A 77 GHz monolithic IMPATT transmitter in standard CMOS technology. In *IEEE MTT-S Int. Microwave Symp. Dig.* Long Beach (USA), June 2005.
- [11] AL-ATTAR, T., LEE, T. H. Monolithic integrated millimeter-wave IMPATT transmitter in standard CMOS technology. *IEEE Trans. on MTT*, 2005, vol. 53, no. 11, p. 3557-3561.
- [12] AL-ATTAR, T. CMOS diodes operating beyond avalanche frequency. In *12<sup>th</sup> Int. Symp. on Quality Electronic Design (ISQED)*. March 14-16, 2011, p. 1-6.
- [13] VYAS, H. P., GUTMANN, R. J., BORREGO, J. M. Leakage current enhancement in IMPATT oscillator by photo-excitation. *Electron. Lett.*, 1977, vol. 13, 189-190.
- [14] VYAS, H. P., GUTMANN, R. J., BORREGO, J. M. Effect of hole versus electron photocurrent on microwave-optical interactions in impatt oscillators. *IEEE Transactions on Electron Devices*, 1979, vol. 26, no. 3, p. 232-234.
- [15] YEN, H. W., BARNOSKI, M. K., HUNSPERGER, R. G., MELVILLE, R. T. Switching of GaAs IMPATT diode oscillator by optical illumination. *Appl. Phys. Lett.*, 1977, vol. 31, p. 120-121.
- [16] SCHWEIGHART, A., VYAS, H. P., BORREGO, J. M., GUTMANN, R. J. Avalanche diode structure suitable for microwave-optical interaction. *Solid-State Electron.*, 1978, vol. 21, p. 1119 to 1121.
- [17] FORREST, J. R., SEEDS, A. J., Optical injection locking of impatt oscillators. *Electronics Letters*, 1978, vol. 14, no. 19, p. 626-627.
- [18] SEEDS, A. J., AUGUSTO, A. Optical control of microwave semiconductor devices. *IEEE Trans. on Microwave Theory and Techniques*, 1990, vol. 38, no. 5, p. 577-585.
- [19] MUKHERJEE, R., BANERJEE, J. P. Effect of electron and hole dominant photocurrent on the millimeter-wave properties of Indium Phosphide Impatt diode at 94 GHz. *Semiconductor Science and Technology*, 1994, vol. 9, p. 1-4.
- [20] MUKHERJEE, M., MAJUMDER, N. Optically illuminated 4H-SiC terahertz IMPATT device. *Egypt J. Solids*, 2007, vol. 30, no. 1, p. 87-101.
- [21] MUKHERJEE, M., MAJUMDER, N., ROY, S. K. Prospects of 4H-SiC double drift region IMPATT device as a photo-sensitive high power source at 0.7 Terahertz frequency regime. *Active and Passive Electronic Components*, 2008, vol. 2008, p. 1-9.
- [22] MUKHERJEE, N., ROY, S. K. Optically modulated III-V nitride-based top-mounted and flip-chip IMPATT oscillators at terahertz regime: Studies on the shift of avalanche transit time phase delay due to photogenerated carriers. *IEEE Trans. on Electron Devices*, 2009, vol. 56, no. 7, p. 1411-1417.
- [23] BANERJEE, S., CHAKRABARTI, P., BAIDYA, R. Studies on frequency chirping in optical illuminated  $\alpha$ -gallium nitride IMPATT diodes at sub-millimeter wave frequency. *Journal of Telecommunication*, 2010, vol. 3, no. 2, p. 1-8.
- [24] BANERJEE, S., BANERJEE, J. P. Studies on optical modulation of III-V GaN and InP based DDR IMPATT diode at sub-millimeter wave frequency. *International Journal of Engineering Science & Technology*, 2010, vol. 2, no. 7, p. 2790-2801.
- [25] MUKHOPADHYAY, J., BANERJEE, S., BANERJEE, J. P. A comparative study on indium phosphide and  $\alpha$ -gallium nitride based IMPATT oscillators for terahertz communication. *Journal of Telecommunications*, 2010, vol. 3, no. 1, p. 14-21.
- [26] ACHARYYA, A., BANERJEE, J. P. A comparative study on the effect of optical illumination on  $\text{Si}_{1-x}\text{Ge}_x$  and Si based DDR IMPATT diodes at W-band. *Iranian Journal of Electronics & Electrical Engineering*, 2011, vol. 7, no. 3, p. 179-189.
- [27] ACHARYYA, A., BANERJEE, J. P. Analysis of photo-irradiated double-drift region silicon impact avalanche transit time devices in the millimeter-wave and terahertz regime. *Terahertz Science and Technology*, 2012, vol. 5, no. 2, p. 97-113.
- [28] ACHARYYA, A., BANERJEE, J. P. Dependence of avalanche response time on photon flux incident on DDR silicon IMPATT

- devices. In *The 32nd PIERS*. Moscow (Russia), August 19-23, 2012, p. 1-6.
- [29] ACHARYYA, A., BANERJEE, J. P. A proposed lateral DDR IMPATT structure for better millimeter-wave optical interaction. In *IEEE Int. Conference on Devices, Circuits and Systems*. Coimbatore (Tamil Nadu, India), 15-16 March 2012, p. 599-602.
- [30] GRANT, W. N. Electron and hole ionization rates in epitaxial silicon. *Solid State Electron*, 1973, vol. 16, no. 10, p. 1189-1203.
- [31] CANALI, C., OTTAVIANI, G., QUARANTA, A. A. Drift velocity of electrons and holes and associated anisotropic effects in silicon. *J. Phys. Chem. Solids*, 1971, vol. 32, no. 8, p. 1707.
- [32] Electronic Archive: *New Semiconductor Materials, Characteristics and Properties*. <http://www.ioffe.ru/SVA/NSM/Semicond>.
- [33] SZE, S. M., RYDER, R. M. Microwave avalanche diodes. *Proc. of IEEE, Special Issue on Microwave Semiconductor Devices*, 1971, vol. 59, no. 8, p. 1140-1154.
- [34] ROY, S. K., SRIDHARAN, M., GHOSH, R., PAL, B. B. Computer methods for the dc field and carrier current profiles in impatt devices starting from the field extremum in the depletion layer. In *Proc. of NASECODE-I Conf. on Numerical Analysis of Semiconductor Devices*. Dublin: Boole Press, 1979, p. 266-274.
- [35] ROY, S. K., BANERJEE, J. P., PATI, S. P. A computer analysis of the distribution of high frequency negative resistance in the depletion layers of IMPATT diodes. In *Proc. of NASECODE-IV Conf. on Numerical Analysis of Semiconductor Devices*. Dublin: Boole Press, 1985, p. 494-500.
- [36] GUMMEL, H. K., BLUE, J. L. A small-signal theory of avalanche noise in IMPATT diodes. *IEEE Trans. on Electron Devices*, 1967, vol. 14, no. 9, p. 569-580.
- [37] NEAMEN, D. A. *Semiconductor Physics and Devices*. The McGraw Hill Companies, 2007, p. 613-615.
- [38] VARSHNI, Y. P. Temperature dependence of the energy gap in semiconductors. *Physica*, 1967, vol. 34 p. 149-154.
- [39] RAJKANAN, K., SINGH, R., SHEWCHUN, J. Absorption coefficient of silicon for solar cell calculations. *Solid-State Electron.*, 1979, vol. 22, p. 793-795.
- [40] BUCHER, K., BRUNS, J., WAGEMANN, H. G. Absorption coefficient of silicon: An assessment of measurements and the simulation of temperature variation. *J. Appl. Phys.*, 1994, vol. 75, no. 2, p. 1127-1131.
- [41] LUY, J. F., CASEL, A., BEHR, W., KASPER, E. A 90-GHz double-drift IMPATT diode made with Si MBE. *IEEE Trans. Electron Devices*, 1987, vol. 34, p. 1084-1089.
- [42] HUSAIN, K., AL-ATTAR, T. CMOS IMPATT impedance and design parameters for millimeter-wave application. *International Journal of Electronics*. Accepted, publication schedule: 2012.
- [43] BAZKIR, O. Quantum efficiency determination of unbiased silicon photodiode and photodiode based trap detectors. *Rev. Adv. Mater. Sci.*, 2009, vol. 21, p. 90-98.

### About Authors...

**Aritra ACHARYYA** received his M. Tech. degree from the Institute of Radio Physics and Electronics, University

of Calcutta, Kolkata, W.B., India. Earlier he obtained his B. E. degree from Bengal Engineering and Science University, Shibpur, Howrah, W.B., India. Presently he has been working as Assistant Professor in the S. K. F. G. I., Sir J. C. Bose School of Engineering, Mankundu, Hooghly, W. B., India since 2011. He is the recipient of Pareshlal Dhar Bhowmik book award in the year 2010 for securing highest marks in M. Tech. (Radio Physics and Electronics) Examination 2010 of University of Calcutta. His research interest is millimeter-wave and terahertz semiconductor devices, more specifically IMPATT devices. He is the principle co-author of more than 40 research papers in different national and international journals and conference proceedings.

**Suranjana BANERJEE** received her B. Sc (Hons.) degree in Electronics in 2002 from the University of Calcutta, India and topped the merit list. She received her B.Tech and M.Tech. degrees from the Institute of Radio Physics and Electronics, University of Calcutta, Kolkata, W.B., India. in 2005 and 2008 respectively. Presently she has been working as Assistant Professor in Academy of Technology, an Engineering college at Adisaptagram, Hooghly 712121, West Bengal, India under West Bengal University of Technology. She has been carrying out research work in the area of both homo-junction and hetero-junction ATT devices under CW and pulsed operations at millimeter wave and terahertz frequency bands. She has published some papers in referred journals and conference proceedings.

**Professor (Dr.) J. P. BANERJEE** obtained B. Sc. (Hons.) and M.Sc. in Physics and Ph. D. in Radio Physics and Electronics, all from the University of Calcutta. He joined the Department of Electronic Science, University of Calcutta in 1989 as a Reader. He has been working as a Professor in the Institute of Radio Physics and Electronics, C.U. since 1998. He is the recipient of prestigious Indian National Science Academy Award of a visiting fellowship. He was awarded Griffith Memorial Prize in Science of the University of Calcutta for being adjudged as the best thesis submitted by him to the University in the year, 1986. He has co-authored more than 170 research papers published in international referred journals as well as conference proceedings in the fields of semiconductor science and technology, microwave and millimeter-wave avalanche transit time devices and avalanche photo detectors. He was the Director of Centre of Millimeter wave Semiconductor Devices and Circuits (CMSDS), a research centre of the University of Calcutta in collaboration with Defense research and Development Organization (DRDO) Government of India, New Delhi during 2008-2010. He guided many students for their doctoral theses in the field of Micro-wave and Millimeter wave devices. He authored many text books for the undergraduate and postgraduate students of Electrical and Electronics Engineering.